DEUTSCHES ELEKTRONEN-SYNCHROTRON DESY

DESY 79/28
May 1979

TRANSVERSE MOMENTA OF HADRONICALLY PRODUCED HEAVY QUARK SYSTEMS: $2 \to 3$ PROCESSES IN QCD

by

Z. Kunszt, E. Pietarinen, and E. Reya

NOTKESTRASSE 85 · 2 HAMBURG 52

To be sure that your preprints are promptly included in the
HIGH ENERGY PHYSICS INDEX ,
send them to the following address (if possible by air mail) :

DESY
Bibliothek
Notkestrasse 85
2 Hamburg 52
Germany

Transverse Momenta of Hadronically Produced Heavy Quark Systems: 2 → 3 Processes in QCD

Z. Kunszt[+], E. Pietarinen, and E. Reya

Deutsches Elektronen-Synchrotron DESY, Hamburg

+ Permanent address: Eötvös University, Budapest.

Abstract

Transverse momentum spectra are calculated for heavy quarkonia $Q\bar{Q}$ (J/ψ, Υ) produced in pp and $\bar{p}p$ collisions. These transverse momenta result from the hard quark (q) and gluon (g) subprocesses $q\bar{q} \to Q\bar{Q}g$, $gq \to Q\bar{Q}q$ and $gg \to Q\bar{Q}g$. The p_T distributions for J/ψ production are expected to be significantly steeper than for the $\mu^+\mu^-$ continuum, whereas the two distributions become similar in the Υ mass region. These effects are partly confirmed by recent ISR measurements. Predictions for $\bar{p}p$ collisions at $\sqrt{s}$ =54o GeV are also given.

Recent measurements [1] of the dimuon spectrum near the Υ region in proton-nucleus scattering at $\sqrt{s}$ = 27.4 GeV have revealed that the mean transverse momentum of the Υ is significantly higher than the corresponding value for the (Drell-Yan) dimuon continuum, the latter being independent of the dimuon mass M above 5 GeV. Typically, $\langle p_T \rangle_\Upsilon$ is about 20 % larger than the continuum value $\langle p_T \rangle_{\mu^+\mu^-}$. Similar effects have been found in the J/ψ region [2,3] and, although inferior in statistics, ISR measurements [4] might also be consistent with this observed trend of the p_T spectrum off and on resonance. A priori, possible differences in the p_T-distributions on and off resonance are not unexpected since in QCD the production mechanisms for heavy quarkonia ($Q\bar{Q}$) states and continuum dimuons are fundamentally different: Whereas the lowest order subprocesses for producing a muon-pair at $p_T \neq 0$ are $q\bar{q} \to \mu^+\mu^- g$ and $gq \to \mu^+\mu^- q$, the leading contribution to the transverse momentum of a given quarkonium state comes from the purely hadronic $2 \to 3$ processes $q\bar{q} \to Q\bar{Q}g$, $gq \to Q\bar{Q}q$ and $gg \to Q\bar{Q}g$, where the light and heavy quarks are denoted by q = u,d,s and Q = c,b,..., respectively, and g stands for the gluon. Because of the complexity of calculating $2 \to 3$ subprocesses (keeping $m_Q \neq 0$), no serious attempt has been made so far to investigate the effects of hard gluon bremsstrahlung for the p_T spectra of quarkonia (charmonium, bottonium, etc.) as compared to the one of the familiar Drell-Yan dimuons. It is the purpose of this article to discuss and calculate these typical QCD effects and to compare them with recent measurements of hadronically produced heavy quarkonia.

Before discussing the more involved case of transverse momenta of quarkonia, let us first briefly recapitulate the situation of the familiar Drell-Yan process. To order α_s the transverse momenta of massive lepton-pairs are

due to the two subprocesses [5-8] shown in Fig. 1. The cross section for dimuon production from initial hadrons A and B is obtained by convoluting the expressions for these subprocesses with the relevant parton distributions

$$\frac{d^2\sigma^{AB}}{dM\,dp_T^2} = \int dx_a\,dx_b\,f_a^A(x_a,q^2)\,f_b^B(x_b,q^2)\,\frac{d^2\sigma^{ab}}{dM\,dp_T^2} \qquad (1)$$

where all color factors are included in $d\sigma^{ab}$ which denotes the subprocess ($q\bar{q}\to\mu^+\mu^-g$ and $gq\to\mu^+\mu^-q$) cross section [6,7,9] for producing a dimuon pair with mass $M\equiv\sqrt{q^2}$ and transverse momentum p_T from partons a and b. The predicted p_T distributions at c.m. rapidity $y = 0$ differ only insignificantly from the y-averaged ones as given in Eq. (1). For our calculations we shall employ throughout the fully renormalization group improved QCD "counting rule-like" quark and gluon distributions $f_a^A(x_a,q^2)$ of Ref. 10. Since the subprocess cross sections $d\sigma^{ab}/dp_T^2$ in Eq. (1) diverge as $p_T \to 0$ (i.e., parallel emission) there is some controversy as to what theoretical quantity should be confronted with experiment. Comparing directly the predictions of Eq. (1) with experiment, one finds [7,9] a reasonable agreement with the shape of the measured p_T distribution for $p_T \gtrsim 1$ GeV. On the other hand, comparing average dimuon transverse momenta [6,11] with experiment, i.e. p_T-moments $\langle p_T\rangle$ and $\langle p_T^2\rangle$ as calculated from Eq. (1) which weigh the small p_T region of $d\sigma/dp_T^2$, yields contradicting results as to the size and importance of the intrinsic transverse momenta k_T of the initial quarks and gluons in Eq. (1) which, so far, are not predictable dynamically by QCD. Values for $\langle k_T\rangle$ between [11] 200 MeV and [6] 800 MeV have been suggested. Although only p_T-moments are well behaved [5] (finite) and therefore the prescription for calculating $\int p_T^n \frac{d\sigma^{ab}}{dp_T^2} dp_T^2$ for $n \gtrsim 1$ is unambiguous, the integration down to small p_T is delicate; α_s becomes substantially different and so

may the scale breaking effects in the parton distributions f_a^A.

Since $d^2\sigma^{ab}/dM\,dp_T^2$ will contain terms like $\log M^2/p_T^2$, the naive "hard scattering" perturbation theory in Eq. (1) breaks down for $p_T \ll M$ and one must sum [12] these logs to all orders in α_s. Going beyond this double logarithmic approximation, [12] Parisi and Petronzio [13] have recently resummed even these double logarithms for the $q\bar{q}$ process and thus were able to compute the whole p_T distribution, including $p_T \simeq 0$, from first principles for large values of the c.m. energy s. The remaining discrepancy between these asymptotic predictions and present measurements at $\sqrt{s} = 27.4$ GeV then implies for the average intrinsic transverse momentum of partons to be $\langle k_T \rangle \simeq 500$ MeV. Since, in the present context, we are mainly interested in the <u>difference</u> between the shape (slope) of the p_T-spectrum of dimuons and quarkonia, which is little influenced by the (common) size of intrinsic transverse momenta, we shall only concentrate on the explicit p_T-distribution $d\sigma/dp_T^2$ for $p_T \gtrsim 1$ GeV, thus avoiding any complicacies due to soft (collinear) gluon emission.

Within the framework of QCD, the production of heavy quark flavors in hadronic collisions is assumed to proceed via the fundamental subprocesses [14-18] $q\bar{q} \to Q\bar{Q}$ and $gg \to Q\bar{Q}$. In this way one can predict [18,19] even absolute cross sections for J/ψ, ψ', Υ, Υ', ... production in fair agreement with experiment. Apart from these lowest order α_s^2 contributions to the total production cross section, the transverse momenta of bound heavy quark states $Q\bar{Q}$ originate from hard gluon radiation off the initial and final quark states as well as off the intermediate gluon, and are thus at least of order α_s^3, namely $q\bar{q} \to Q\bar{Q}g$, $gq \to Q\bar{Q}q$ and $gg \to Q\bar{Q}g$ as shown in Fig. 2. The p_T distribution of

the $Q\bar{Q}$ system is then formally given by a similar expression as in Eq. (1) but integrated over the invariant energy $M \equiv \sqrt{q^2}$ of the $Q\bar{Q}$ system

$$\frac{d\sigma^{AB}}{dp_T^2} = \int_{2m_Q}^{2m_o} dM \; \frac{d^2\sigma^{AB}}{dM\, dp_T^2} \tag{2}$$

where for the coupling of the fundamental subprocesses we always take $\alpha_s = 12\pi/23 \ln(M^2/\Lambda^2)$ with $\Lambda \simeq 0.5$ GeV. Within the semi-local duality approach [15,16,19] the upper limit of integration $2m_o$ should correspond to the threshold for open flavor Q production ($D\bar{D}$, etc.), i.e., $2m_o = 2m_D$ for charmonium and $2m_o \simeq 10.4$ GeV for bottonium. Furthermore, to obtain the absolute cross section for producing a definite $Q\bar{Q}$ bound state, the partonic cross sections in Eq. (2) should be divided [19] by the number of bound $Q\bar{Q}$ levels in the invariant $Q\bar{Q}$ mass interval M considered. Alternatively, one might also use [17] $2m_o = \sqrt{s}$ and/or employ only color singlet projections [14,18] of the gluonic amplitudes, i.e., the quarkonia ground states are supposed to be dominantly produced via p-wave resonances. Since, in the present context, we are not interested in this detailed model assumptions, we shall state all our results with the normalization corresponding to Eq. (2); of course, if one wants to compare these results with measured <u>absolute</u> cross sections, they have to be multiplied by the appropriate duality (bound state) division factors and by appropriate branching ratios. However, such ambiguities as well as the specific choice of α_s and of the heavy quark mass m_Q, and the detailed structure of parton distributions affect mainly the absolute normalization of cross section, but are of little influence as far as the shapes (slopes) of the p_T distributions $d\sigma/dp_T^2$ are concerned. The important point of our investigation is to study the p_T distribution in Eq. (2) on-resonance <u>relative</u>

to the one of the continuum dimuons in Eq. (1): This possible difference between the dimuon and the $Q\bar{Q}$ p_T-spectrum should be entirely due to dynamical QCD effects and is also independent of intrinsic parton k_T's.On the other hand, at the present state of art, we cannot calculate "uniquely" the p_T-moments directly since their definition involves total cross sections. This is, because order α_s^3 contributions to the leading order α_s^2 total cross section come not only from the diagrams of fig. 2 but also from the so far unknown virtual gluon-loop corrections to the leading $q\bar{q} \to Q\bar{Q}$ and $gg \to Q\bar{Q}$ subprocesses. However, it should be emphasized that the cleanest test of effects due to hard gluon radiation would be to compare directly the p_T distribution for $p_T \gtrsim 1$ GeV, and not just averaged quantities.

A detailed discussion of the calculation of the massless $2 \to 3$ scattering processes in QCD has been given in Ref. 20, where also a comparison of their relative magnitudes as well as their importance relative to the $2 \to 2$ subprocess can be found. The invariant matrix elements have been calculated using the algebraic computer program [21] REDUCE. The complexity of the calculation increases with the number of gluon lines since, unlike in QED, only physical transverse helicities have to be kept in the gluon polarization sum or instead one has to use a covariant (Feynman) gauge and add the contributions of ghost diagrams. Using this latter procedure, there are 5 Feynman diagrams for each process of Fig. 2 (a) and (b), whereas the $gg \to Q\bar{Q}g$ subprocess in Fig. 2 (c) consists of 16 $ggg Q\bar{Q}$ Feynman diagrams and 5 ghost diagrams; thus we had to calculate 25 Cutkosky diagrams for each Fig. 2 (a) and (b), and 281 Cutkosky diagrams for Fig. 2 (c). The heavy quark masses m_Q for the diagrams in Fig. 2 have been taken to be $m_c = 1.25$ GeV and $m_b = 4.5$ GeV. In order to avoid infrared singularities the differential cross sections have

been calculated with a cut in the transverse momentum of the produced heavy quark, $p_T \geq 1$ GeV. We have checked our algebraic calculations by an entirely independent numerical procedure using helicity projectors. For further details and explicit analytic expressions of the fundamental cross sections we refer the interested reader to the Appendix.

In Figs. 3 and 4 show our predictions for $d\sigma/dp_T^2$ at $\sqrt{s}$ = 27.4 GeV and 63 GeV together with the existing data of Ref. 22 and Refs. 4 and 23, respectively. For comparison we also show $d^2\sigma/dM\,dp_T^2$ of the continuum in the appropriate dimuon mass region according to the graphs of Fig. 1. Again it should be emphasized that, as already discussed, only the p_T shapes can be safely calculated for $p_T \gtrsim 1$ GeV, whereas the absolute normalizations suffer from uncertainties such as the q^2-dependent gluon wave functions, the choice of α_s, and from the details of the duality model assumptions for Eq. (2). As a general rule, the contributions to the p_T spectrum from the $q\bar{q}$ and gg subprocesses are always steeper than the contribution of gq scattering. Therefore, at <u>small</u> values of $\sqrt{\tau} \equiv M/\sqrt{s}$ where the gg subprocess gives a sizeable contribution we expect a different (steeper) p_T distribution for resonance production than for the $\mu^+\mu^-$ continuum where no gg subprocess exists in leading order. These effects are clearly seen in the J/ψ mass region shown in Figs. 3 and 4 where the predicted p_T spectrum on resonance (solid curve) is significantly steeper than off resonance (dotted curve). The larger the energy becomes, i.e. the larger the steep contribution from the gg process becomes relative to the gq subprocess, the more pronounced this effect will be. At ISR energies, Fig. 4, the transverse momentum distribution of J/ψ production is significantly steeper (solid curve) than for the production of lepton pairs of similar mass (dotted curve):

The recent J/ψ measurements at ISR[4] appear to follow our predictions due to the diagrams in Fig. 2, and seem to disagree with the flatter p_T spectrum predicted for the $\mu^+\mu^-$ continuum stemming from the graphs in Fig. 1.

On the other hand at <u>larger</u> values of $\sqrt{\tau}$, as is the case in the Υ mass region for example, the gg as well as the $q\bar{q}$ subprocesses will be strongly suppressed because of the decreasing gluon and antiquark wave functions for increasing values of[24] $\sqrt{\tau}$. Thus the $gq \to Q\bar{Q}q$ subprocess will be mainly responsible for the p_T spectrum on resonance which should therefore be similar to the p_T shape off resonance dominated by a similar process $gq \to \mu^+\mu^-q$. Our predictions in Figs. 3 and 4 in the Υ mass region show that this behavior is indeed the case and that the difference in the p_T shape on and off resonance, which is so distinct in the J/ψ region, disappears. Recent ISR data seem to confirm[23] the similarity of the p_T spectra of the $\mu^+\mu^-$ continuum and of Υ production. We therefore expect in general that the average momentum increases for increasing quarkonia mass since the p_T distributions become flatter. Indeed this trend has also been observed experimentally[1,2,4] where for instance at ISR energies it has been found[4] that $\langle p_T \rangle_{J/\psi} = (1.2 \pm 0.04)$ GeV and $\langle p_T \rangle_{\Upsilon} = (1.67 \pm 0.18)$ GeV. Additional precision measurements of the p_T spectra on and off resonance in the J/ψ as well as Υ mass region should provide us with a clean test of the two different production mechanisms for heavy quark bound states and for dimuons and for the different hard scattering processes in Fig. 2 and 1, respectively, responsible for their p_T distributions.

Apart from the absolute normalization, the p_T spectra on and off resonance will be always the same if one adopts the simple minded approach of Ref. 25

to calculate $d\sigma/dp_T^2$ for resonance and $\mu^+\mu^-$ continuum production using the same two (massless) subprocesses responsible for transverse dimuon production as shown in Fig. 1. Needless to say, that this approach lacks any theoretical basis within the framework of perturbation theory and QCD.

In order to check the sensitivity of our results to the special choice of parton distributions, we have repeated the calculations by turning off the q^2-dependence of the parton densities in Eq. (1), i.e. by setting q^2 in $f_a^A(x,q^2)$ equal to the input momentum[10] $Q_o^2 = 1.8$ GeV^2. Since the gluon initiated subprocesses enter dominantly our predictions we also have repeated the calculations using a broad gluon distribution[26] $xG(x,Q_o^2) = 0.8$ $(1+9x)(1-x)^4$ which is much harder than the standard one[10] proportional to $(1-x)^5$. In both cases, all predicted p_T distributions in Figs. 3 and 4 become flatter by at most 10 % but the differences of the p_T shapes on and off resonance remain unchanged. On the other hand the absolute normalization of the cross sections shown will of course significantly change (typically they will increase by a factor 2-10 depending on the reaction and on the kinematical region considered), but these are sensitive also to other uncertainties as already discussed extensively. Furthermore we also repeated the calculation using the color singlet[14] projections of the quarkonia production cross sections in Fig. 2(b) and (c); in this case the quarkonia ground states $J/\psi, \Upsilon$ etc. are expected to be dominantly produced in association of photons via p-waves. In this case the p_T slopes become even steeper on resonance by about 15 % than those shown in Figs. 3 and 4, and thus the difference between the p_T slopes of the J/ψ and the corresponding $\mu^+\mu^-$ continuum will be even more pronounced. The absolute normalization

for this model would then be smaller by a factor of 5-8.

Although at the present state of art one cannot calculate reliably p_T-moments of heavy quarkonia, we parametrize our predicted cross sections by $d\sigma/dp_T^2 \sim \exp(-b\,p_T)$ which is valid in a limited p_T region only, say, $1.5 \lesssim p_T \lesssim 3$ GeV, from which we might deduce the behavior of $\langle p_T \rangle = 2/b$ for the various processes considered. However, it should be emphasized that this method[4] for calculating the average p_T should be taken with caution since $\langle p_T \rangle$ is sensitive to the small p_T region only where non-perturbative intrinsic k_T smearing effects and $O(\alpha_s^3)$ loop corrections could change even the relative $\langle p_T \rangle$ of the various processes. Nonetheless, we show the results for b in Table I for quarkonia production as compared to the Drell-Yan continuum for pp as well as $\bar{p}p$ scattering. For pp scattering we see that the p_T spectrum of J/ψ is similar to the one of $\mu^+\mu^-$ and both become flatter, i.e. p_T increases, for increasing energy $\sqrt{s}$. In the Υ mass region, however, the Υ has a flatter spectrum than the $\mu^+\mu^-$ continuum for $\sqrt{s} \lesssim 30$ GeV, whereas at larger (ISR) energies the two spectra become similar: at $\sqrt{s} = 27.4$ GeV we expect $\langle p_T \rangle_\Upsilon^{pp}$ to be about 10 % larger than $\langle p_T \rangle_{\mu^+\mu^-}^{pp}$, whereas $\langle p_T \rangle_\Upsilon^{pp} \simeq \langle p_T \rangle_{\mu^+\mu^-}^{pp}$ for larger (ISR) energies, which is consistent with experiment.[1,4] For $\bar{p}p$ scattering, however, the b values for J/ψ production are always larger than those of the $\mu^+\mu^-$ continuum and therefore we expect $\langle p_T \rangle_{J/\psi}^{\bar{p}p}$ to be smaller than $\langle p_T \rangle_{\mu^+\mu^-}^{\bar{p}p}$ by about 15 % especially for $\sqrt{s} \lesssim 50$ GeV which is consistent with experiment.[3] On the other hand, in the Υ mass region we expect $\langle p_T \rangle_\Upsilon^{\bar{p}p} \simeq \langle p_T \rangle_{\mu^+\mu^-}^{\bar{p}p}$ throughout the whole energy range considered. Table I also shows, as already discussed, that using only color singlet amplitudes of the gluon initiated reactions for quarkonia production,[14] one expects a somewhat steeper p_T

distribution.

Finally, in Fig. 5 we give predictions for the p_T distributions of $\bar{p}p$ scattering in the Υ mass region at $\sqrt{s}$ = 540 GeV. In addition to the flat contribution from the gq subprocess, the steeper gg subprocess contributes a sizeable fraction (since $\sqrt{\tau} \simeq 0.02$) and therefore the p_T distribution on resonance is expected to be significantly steeper than the one off resonance $(\mu^+\mu^-)$, the latter being dominated by the $gq \to \mu^+\mu^- q$ subprocess. Again, it would be interesting to see whether this distinct difference in the p_T shapes will be confirmed experimentally. Since the $gq \to b\bar{b}q$ and $gg \to b\bar{b}g$ subprocesses dominate throughout the whole p_T region (and not $q\bar{q} \to b\bar{b}g$), the predicted total p_T distribution on resonance is identical in shape and absolute normalization for pp collisions, whereas off resonance $(\mu^+\mu^-)$ the p_T shape is somewhat flatter than the dotted curve shown in Fig. 5.

Appendix

Here we shall give the explicit analytic expressions for $d\hat{\sigma}^{ab}$ of the fundamental parton scattering processes which are required in Eqs. (2) and (1) to calculate $d\sigma^{AB}/dp_T^2$ for heavy quarkonia production. To leading order in perturbative QCD, the differential cross section for the production of a massive $Q\bar{Q}$ pair with a hard gluon emission

$$q(-k_4) + \bar{q}(-k_5) \to \bar{Q}(k_1) + Q(k_2) + g(k_3) \tag{A1}$$

can we written as

$$\frac{d^2\hat{\sigma}^{q\bar{q}}}{dM\,dp_T^2} = \frac{\alpha_s^3}{4\pi\hat{s}} \sqrt{\frac{M^2 - 4m_Q^2}{(\hat{s}-M^2)^2 - 4\hat{s}p_T^2}} \frac{1}{36} \int d\Omega_{TY}\, W(\{x_{ij}\}, m_Q^2) \tag{A2}$$

where $q(-k_4)$ and $\bar{q}(-k_5)$ denote massless quarks with outgoing momenta k_4 and k_5, $\bar{Q}$ and Q are the final massive quarks with momenta k_1 and k_2 and mass m_Q, g is the final gluon with momentum k_3. The invariant mass of the massive quark pair is denoted by M

$$q^2 = (k_1 + k_2)^2 \quad , \quad M \equiv \sqrt{q^2} \quad . \tag{A3}$$

The transverse momenta of the quark pair $Q\bar{Q}$ are $\vec{p}_T \equiv \vec{q}_T = (\vec{k}_1 + \vec{k}_2)_T$, and $\hat{s} = (k_4 + k_5)^2$, and the factor 1/36 is due to averaging over the initial spin and color states. $d\Omega_{TY}$ denotes the integration over the Treiman-Yang angles (see Fig. 6) defined, in the frame $\vec{q} = 0$, via the relations

$$\cos\theta_{TY} = -\left.\frac{\vec{k}_2\cdot\vec{k}_5}{|\vec{k}_2|\,|\vec{k}_5|}\right|_{\vec{q}=0} , \qquad \cos\phi_{TY} = -\left.\frac{(\vec{k}_5\times\vec{k}_2)\cdot(\vec{k}_5\times\vec{k}_3)}{|\vec{k}_5\times\vec{k}_2|\,|\vec{k}_5\times\vec{k}_3|}\right|_{\vec{q}=0} . \tag{A4}$$

The function $W(\{x_{ij}\}, m_Q^2)$ in Eq. (A2) is the invariant matrix element squared of the process. It is a rational function of the variables

$$x_{ij} = 2\,k_i\cdot k_j \quad , \qquad i,j = 1,\ldots,5 \tag{A5}$$

and m_Q^2. In particular, for the subprocess (A1) we can write

$$W(\{x_{ij}\}, m_Q^2) = \sum_{i,j=1}^{5} C_{ij}\, A_{ij}(\{x_{ij}\}, m_Q^2) \tag{A6}$$

where C_{ij} is a real symmetric matrix of color factors

$$C = \frac{1}{3}\begin{pmatrix} 8 & 1 & 9 & -2 & -7 \\ & 8 & 9 & -7 & -2 \\ & & 18 & -9 & -9 \\ & & & 8 & 1 \\ & & & & 8 \end{pmatrix} \tag{A7}$$

and the matrix elements $A_{ij}(\{x_{ij}\}, m_Q^2)$ are given by the equation

$$A_{ij} = \sum_{\substack{\text{initial, final} \\ \text{spins}}} T_i\, T_j^* \quad , \qquad i,j = 1,\ldots,5 \tag{A8}$$

where the T_i's denote the Lorentz part of the amplitudes defined by the five Feynman diagrams in Fig. 7.

It is convenient to introduce symmetric matrices N_{ij} and D_{ij},

$$A_{ij} = -16 \frac{N_{ij}}{D_{ij}} \tag{A9}$$

which are homogeneous functions of the x_{ij}'s and of m_Q^2. In terms of the variables

$$s_{ij} = (k_i + k_j)^2 = x_{ij} + m_i^2 + m_j^2$$

the denominator matrix D_{ij} in Eq. (A9) has the following form

$$\mathcal{D} = \begin{pmatrix} x_{31}^2 x_{54}^2 & 2x_{23}x_{31}x_{54}^2 & 4s_{12}x_{31}x_{54}^2 & 2s_{12}x_{31}x_{43}x_{54} & 2s_{12}x_{31}x_{53}x_{54} \\ & x_{23}^2 x_{54}^2 & 4s_{12}x_{23}x_{54}^2 & 2s_{12}x_{23}x_{43}x_{54} & 2s_{12}x_{23}x_{53}x_{54} \\ & & 4s_{12}^2 x_{54}^2 & 4s_{12}^2 x_{43}x_{54} & 4s_{12}^2 x_{53}x_{54} \\ & & & s_{12}^2 x_{43}^2 & 2s_{12}^2 x_{43}x_{53} \\ & & & & s_{12}^2 x_{53}^2 \end{pmatrix} \tag{A10}$$

and for the matrix elements N_{ij} we find

$$N_{11} = x_{31}(-x_{42}x_{53} - x_{43}x_{52} + 2m_Q^2 x_{54}) + 2m_Q^2(x_{41}x_{52} + x_{42}x_{51} + x_{42}x_{53} + x_{43}x_{52} + 2m_Q^2 x_{54})$$

$$N_{12} = x_{12}\left[x_{41}(2x_{52}+x_{53}) + x_{42}(2x_{51}+x_{53}) + x_{43}(x_{51}+x_{52}) + 4m_Q^2 x_{54}\right]$$
$$+ x_{23}\left[x_{41}(-2x_{51}+x_{52}) + x_{42}x_{51} + 2m_Q^2 x_{54}\right]$$
$$+ x_{31}\left[x_{41}x_{52} + x_{42}(x_{51}-2x_{52}) + 2m_Q^2 x_{54}\right] - 4m_Q^2 x_{43}x_{53}$$

$$N_{13} = x_{12}\left[-2x_{31}x_{54} + x_{41}(4x_{52}+3x_{53}) + x_{42}(4x_{51}+3x_{53})\right.$$
$$\left. + x_{43}(3x_{51}+3x_{52}+2x_{53}) + 8m_Q^2 x_{54}\right]$$
$$+ x_{23}\left[x_{41}(-6x_{51}+x_{52}-x_{53}) + (x_{42}-x_{43})x_{51} + 4m_Q^2 x_{54}\right]$$
$$+ x_{31}\left[x_{41}x_{52} + x_{42}(x_{51}-2x_{52}-3x_{53}) - 3x_{43}x_{52}\right]$$
$$+ 2m_Q^2\left[x_{41}(2x_{51}+4x_{52}+3x_{53}) + x_{42}(4x_{51}-2x_{52}+5x_{53})\right.$$
$$\left. + x_{43}(3x_{51}+5x_{52}) + 8m_Q^2 x_{54}\right]$$

$$N_{14} = x_{51}(-x_{12}x_{43}+x_{23}x_{41}+x_{42}x_{43}) + x_{31}\left[2x_{41}x_{52} + x_{42}(x_{51}-x_{54}) + 2x_{43}x_{52} + 2m_Q^2 x_{54}\right]$$
$$+ x_{41}\left[2(x_{41}+x_{43})x_{52} + x_{42}(2x_{51}+x_{53}) + 2m_Q^2(x_{53}+2x_{54})\right]$$
$$+ 2m_Q^2 x_{43}(x_{53}+x_{54}-x_{51}-x_{52})$$

$$N_{15} = N_{14}(4 \leftrightarrow 5)\,, \qquad N_{22} = N_{11}(1 \leftrightarrow 2)\,, \qquad N_{23} = N_{13}(1 \leftrightarrow 2)\,,$$
$$N_{24} = N_{14}(1 \leftrightarrow 2)\,, \qquad N_{25} = N_{24}(4 \leftrightarrow 5)$$

$$N_{33} = x_{12}\left[2x_{54}(x_{12}-x_{23}-x_{31}) + x_{41}(-2x_{51}+6x_{52}+5x_{53})\right.$$
$$\left. + x_{42}(-2x_{52}+6x_{51}+5x_{53}) + x_{43}(5x_{51}+5x_{52}+4x_{53}) + 28m_Q^2 x_{54}\right]$$
$$+ x_{23}\left[-2x_{31}x_{54} + x_{41}(-6x_{51}+x_{52}-3x_{53}) + (x_{42}-3x_{43})x_{51}\right]$$
$$+ x_{31}\left[x_{41}x_{52} + x_{42}(x_{51}-6x_{52}-3x_{53}) - 3x_{43}x_{52}\right]$$
$$+ 2m_Q^2\left[x_{41}(-4x_{51}+4x_{52}+7x_{53}) + x_{42}(4x_{51}-4x_{52}+7x_{53})\right.$$
$$\left. + x_{43}(7x_{51}+7x_{52}+2x_{53}) + 24m_Q^2 x_{54}\right]$$

$$
\begin{aligned}
N_{34} = {} & x_{12}\left[x_{54}(x_{23}+x_{31}+x_{42}+x_{41}) - 2x_{43}(x_{51}+x_{52})\right] \\
& + x_{23}\left[2x_{31}x_{54} + x_{41}(x_{52}-x_{53}-x_{54}) + 3x_{51}(x_{42}+x_{43}) + 8m_Q^2 x_{54}\right] \\
& + x_{31}\left[x_{42}(x_{51}-x_{53}-x_{54}) + 3x_{52}(x_{41}+x_{43}) + 8m_Q^2 x_{54}\right] \\
& + x_{41}\left[3(x_{41}+x_{43})x_{52} + x_{42}(x_{51}+x_{52}+2x_{53}) + 2m_Q^2(x_{53}+5x_{54})\right] \\
& + x_{42}\left[3(x_{42}+x_{43})x_{51} + 2m_Q^2(x_{53}+5x_{54})\right] \\
& + 2m_Q^2 x_{43}(2x_{53}+2x_{54}-5x_{51}-5x_{52})
\end{aligned}
$$

$$
N_{44} = x_{43}(-x_{23}x_{51} - x_{31}x_{52} - 2m_Q^2 x_{53})
$$

$$
\begin{aligned}
N_{45} = {} & x_{54}\left[x_{23}(x_{41}+x_{51}) + x_{31}(x_{42}+x_{52}) + 4m_Q^2(x_{53}+x_{54}+x_{43})\right] \\
& + x_{41}\left[x_{52}(x_{43}+2x_{54}) + x_{53}(x_{52}-2x_{42})\right] \\
& + x_{51}\left[-2x_{43}x_{52} + x_{42}(x_{53}+2x_{54}+x_{43})\right]
\end{aligned}
$$

$$
N_{35} = N_{34}(4 \leftrightarrow 5) \quad , \qquad N_{55} = N_{44}(4 \leftrightarrow 5) \quad . \tag{A11}
$$

The cross section for the subprocess

$$
q(-p_4) + g(-p_5) \rightarrow \bar{Q}(p_1) + Q(p_2) + q(p_3) \tag{A12}
$$

can be easily obtained from Eq. (A2) by the use of crossing symmetry: Interchanging the antiquark line with the gluon line, modifying the spin and colour average factor, and introducing a negative overall sign, we get

$$\frac{d^2\sigma^{gq}}{dM\,dp_T^2} = -\frac{\alpha_s^3}{4\pi\tilde{s}}\sqrt{\frac{M^2-4m_Q^2}{(\tilde{s}-M^2)^2-4\tilde{s}p_T^2}}\;\frac{1}{96}\int d\tilde{\Omega}_{TY}\,W(\{x_{ij}\},m_Q^2) \qquad \text{(A13)}$$

where $\tilde{s} = (p_4 + p_5)^2$ and the Treiman-Yang angles are now defined in terms of $\vec{p}_i$, similarly to Eq. (A4), by

$$\cos\tilde{\theta}_{TY} = -\left.\frac{\vec{p}_2\cdot\vec{p}_5}{|\vec{p}_2||\vec{p}_5|}\right|_{\vec{p}_1=-\vec{p}_2}, \qquad \cos\tilde{\phi}_{TY} = -\left.\frac{(\vec{p}_5\times\vec{p}_3)\cdot(\vec{p}_5\times\vec{p}_2)}{|\vec{p}_5\times\vec{p}_3|\,|\vec{p}_5\times\vec{p}_2|}\right|_{\vec{p}_1=-\vec{p}_2}$$

The invariant matrix element squared $W(\{x_{ij}\},m_Q^2)$ is the same function as given by Eqs. (A6 - A11), the physical region of the variables x_{ij}, however, is different: they are defined by Eq. (A5) in terms of the vectors k_i's

$$k_i = p_i \text{ if } i = 1,2,4, \text{ and } k_3 = p_5,\ k_5 = p_3. \qquad \text{(A14)}$$

The algebraic formula obtained for the invariant function $\bar{W}$ for the subprocess

$$g(-l_4) + g(-l_5) \to \bar{Q}(l_1) + Q(l_2) + g(l_3) \qquad \text{(A15)}$$

is exceedingly longer than the expressions given by Eqs. (A6 - A11). In this case we have 16 Feynman diagrams, where 3- and 4-gluon vertices occur more frequently. Furthermore, there are complications due to the summation over the gluon helicities since either a helicity projector has to be used,

$$\sum_{pol}\varepsilon_\mu\varepsilon_\nu = -g_{\mu\nu} + \frac{k_\mu n_\nu + k_\nu n_\mu}{k\cdot n} - \frac{k_\mu k_\nu}{(k\cdot n)^2}, \qquad \text{(A16)}$$

where n_μ is an arbitrary time-like unit vector ($n^2 = +1$), or one can replace the sum $\sum \varepsilon_\mu \varepsilon_\nu$ with $-g_{\mu\nu}$ but then the contributions of ghost diagrams have to be subtracted in order to eliminate the unphysical longitudinal gluon polarization component. In the algebraic calculation with REDUCE it was more convenient to apply the second method. We also calculated the function $\bar{W}(\{x_{ij}\}, m_Q^2)$ at several phase space points with the help of an entirely numerical method, in which the helicity projector (A16) has been used. The virtue of the algebraic expression is obvious: the calculation of the value of the function $\bar{W}$ at a given point with the help of the numerical program was slower by a factor of about 200.

Finally we mention that if we allow to produce the final quark pair only in a color singlet state[14] then we should only change the color matrix in Eq. (A7) to

$$C^{singlet} = \frac{1}{3} \begin{pmatrix} 1 & -1 & 0 & 0 & 0 \\ -1 & 1 & 0 & 0 & 0 \\ 0 & 0 & 0 & 0 & 0 \\ 0 & 0 & 0 & 0 & 0 \\ 0 & 0 & 0 & 0 & 0 \end{pmatrix} . \qquad \text{(A17)}$$

References

1. D.M. Kaplan et al., Phys. Rev. Lett. 40, 435 (1978).

2. J.G. Branson et al., Phys. Rev. Lett. 38, 1331 (1977).

3. K.J. Anderson et al., University of Chicago report EFI 78-38, paper submitted to the XIX Intern. Conf. on High Energy Physics, Tokyo, 1978; and Phys. Rev. Lett. 42 ,944 (1979).

4. C. Kourkoumelis et al., Brookhaven report BNL-25075, paper submitted to the XIX Intern. Conf. on High Energy Physics, Tokyo, 1978.

5. H.D. Politzer, Nucl. Phys. B129, 301 (1977); A.V. Radyushkin, Phys. Lett. 69B, 245 (1977).

6. H. Fritzsch and P. Minkowski, Phys. Lett. 73B, 80 (1978); G. Altarelli, G. Parisi and R. Petronzio, Phys. Lett. 76B, 351 (1978).

7. K. Kajantie and R. Raitio, Nucl. Phys. B139, 72 (1978).

8. For a complete list of references we refer the reader to the review of F. Halzen, in Proceedings of the XIX Intern. Conf. on High Energy Physics, Tokyo, 1978; and Wisconsin report COO-881-53.

9. F. Halzen and D.M. Scott, Phys. Rev. Lett. 40, 1117 (1978); Phys. Rev. D18, 3378 (1978).

10. J.F. Owens and E. Reya, Phys. Rev. D17, 3003 (1978).

11. M. Glück and E. Reya, Nucl. Phys. B145, 24 (1978).

12. Yu. L. Dokshitzer, D.I. D'yakonov and S.I. Troyan, Phys. Lett. 78B, 290 (1978); ibid. 79B, 269 (1978).

13. G. Parisi and R. Petronzio, Ref. TH.2627-CERN (1979).

14. M.B. Einhorn and S.D. Ellis, Phys. Rev. D12, 2007 (1975).

15. H. Fritzsch, Phys. Lett. 67B, 217 (1977).

16. M. Glück, J.F. Owens and E. Reya, Phys. Rev. D17, 2324 (1978).

17. L.M. Jones and H.W. Wyld, Phys. Rev. D17, 2332 (1978).

18. C.E. Carlson and R. Suaya, Phys. Rev. D18, 760 (1978);
Phys. Lett. 81B, 329 (1979).

19. M. Glück and E. Reya, Phys. Lett. 79B, 453 (1978).

20. Z. Kunszt and E. Pietarinen, DESY 79/18 (1979).

21. A.C. Hearn, REDUCE 2, University of Utah report, 1965.

22. K. Ueno et al., Phys. Rev. Lett. 42, 486 (1979).

23. U. Becker, Nordic Particle Physics Meeting, NORDITA, Kopenhagen, April 1979.

24. The dominant contribution to the integral in Eq. (1) comes from the region where $x_a \simeq x_b \simeq \sqrt{\tau}$.

25. F. Halzen, J.P. Leveille and D.M. Scott, University of Wisconsin -
Madison report COO-881-95, April 1979.

26. R.P. Feynman, R.D. Field and G.C. Fox, Phys. Rev. D18, 3320 (1978).

Table 1. Calculated values of b in units of GeV^{-1} according to parametrizing $d\sigma/dp_T^2 \sim \exp(-b\,p_T)$ in the region $1.5 \leq p_T \leq 3$ GeV. It should be kept in mind that the predicted values of b are <u>not</u> constant throughout the whole p_T region and they should be regarded only as an illustration of the <u>relative</u> trend of the QCD predictions for $\langle p_T \rangle$ between resonance (J/ψ, Υ) and continuum ($\mu^+\mu^-$) production as a function of $\sqrt{s}$.

$\sqrt{s}$ (GeV)	pp				$\bar{p}p$				pp (color singlet)	
	J/ψ	($\mu^+\mu^-$)	Υ	($\mu^+\mu^-$)	J/ψ	($\mu^+\mu^-$)	Υ	($\mu^+\mu^-$)	J/ψ	Υ
20.6	2.7	(2.7)	2.6	(3.0)	2.6	(2.4)	2.7	(2.7)	3.1	2.8
27.4	2.4	(2.3)	1.9	(2.1)	2.5	(2.2)	2.1	(2.0)	3.0	2.1
63	2.0	(1.9)	1.6	(1.6)	2.1	(1.9)	1.6	(1.5)	2.5	1.7

Figure Captions

Fig. 1. Lowest-order contributions to transverse dimuon momenta (crossed diagrams are not shown).

Fig. 2. Lowest-order contributions to the transverse momenta of heavy quarkonia $Q\bar{Q}$. There are 5 diagrams for each process in (a) and (b), whereas the subprocess in (c) consists of 16 $ggg Q\bar{Q}$ Feynman diagrams and 5 ghost diagrams.

Fig. 3. QCD predictions (solid curves) for the p_T distributions of J/ψ and Υ production at $\sqrt{s}$ = 27.4 GeV according to the diagrams in Fig. 2. The dashed curves show the contributions of the various subprocesses. The absolute normalizations are as in Eq. (2), but in order to compare with experimentally measured absolute cross sections one has to invoke additional model assumptions as explained in the text. These p_T shapes are compared with the ones of the $\mu^+\mu^-$ continuum $d^2\sigma/dM\,dp_T^2$ (dotted curves) in the appropriate mass regions according to the diagrams of Fig. 1. The Υ production data[22] are normalized to our predictions at p_T = 2 GeV.

Fig. 4. QCD predictions (solid curves) for the p_T distributions of J/ψ and Υ production at ISR energies. The notation and conventions are as in Fig. 3. The J/ψ production data are taken from Ref. 4.

Fig. 5. QCD predictions (solid and dashed curves) for the p_T distribution of Υ production at $\sqrt{s}$ = 540 GeV. Since the gq and gg subprocesses

dominate throughout the whole p_T region, the prediction for the total p_T distribution is the same for pp scattering. For comparison we also show the expected p_T distribution $d^2\sigma/dM\,dp_T^2$ of the Drell-Yan $\mu^+\mu^-$ continuum (dotted curve); for pp collisions this prediction becomes somewhat flatter at large values for p_T (i.e. a factor of 2 smaller at p_T = 70 GeV). The conventions are as in Fig. 3.

Fig. 6. Definition of the Treiman-Yang angles.

Fig. 7. Feynman diagrams for the reaction $q(-k_4)+\bar{q}(-k_5) \rightarrow \bar{Q}(k_1)+Q(k_2)+g(k_3)$ where the heavy quark Q states are denoted by heavy lines.

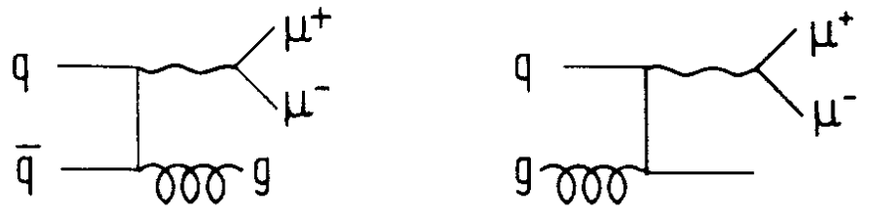

Fig.1

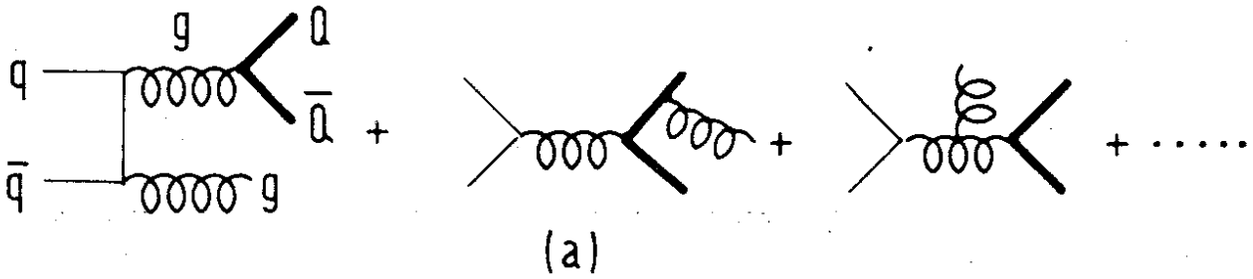

(a)

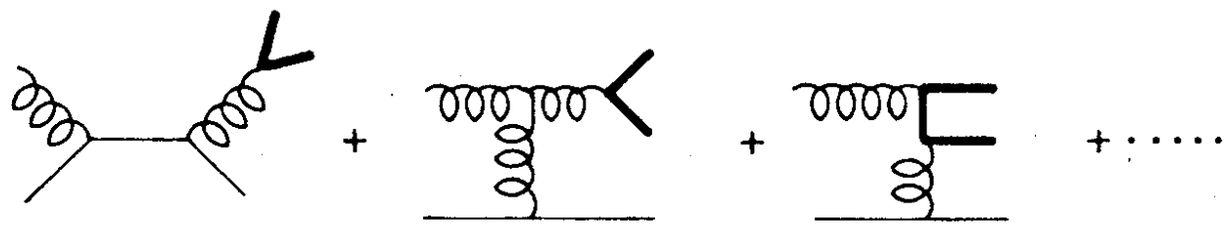

(b)

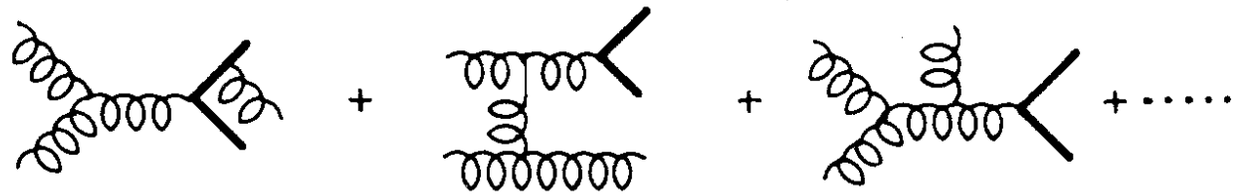

(c)

Fig.2

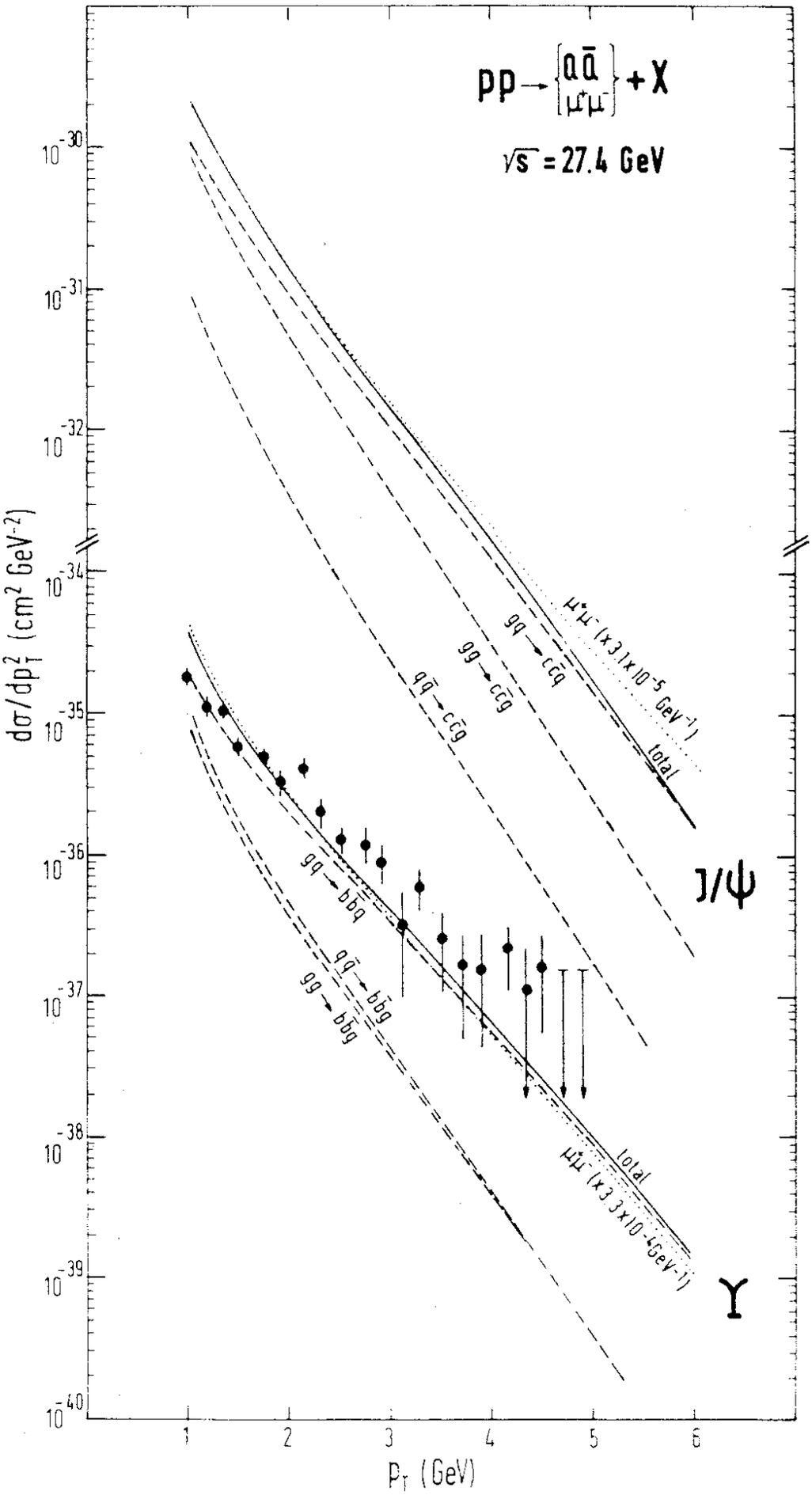
pp → {qq̄ / μ⁺μ⁻} + X
√s = 27.4 GeV
dσ/dp_T² (cm² GeV⁻²)
P_T (GeV)
μ⁺μ⁻ (×3.1×10⁻⁵ GeV⁻¹)
total
gg → cc̄g
qq̄ → cc̄g
J/ψ
gg → bb̄g
qq̄ → bb̄g
μ⁺μ⁻ (×3.3×10⁻⁴GeV⁻¹)
Υ

Fig 2

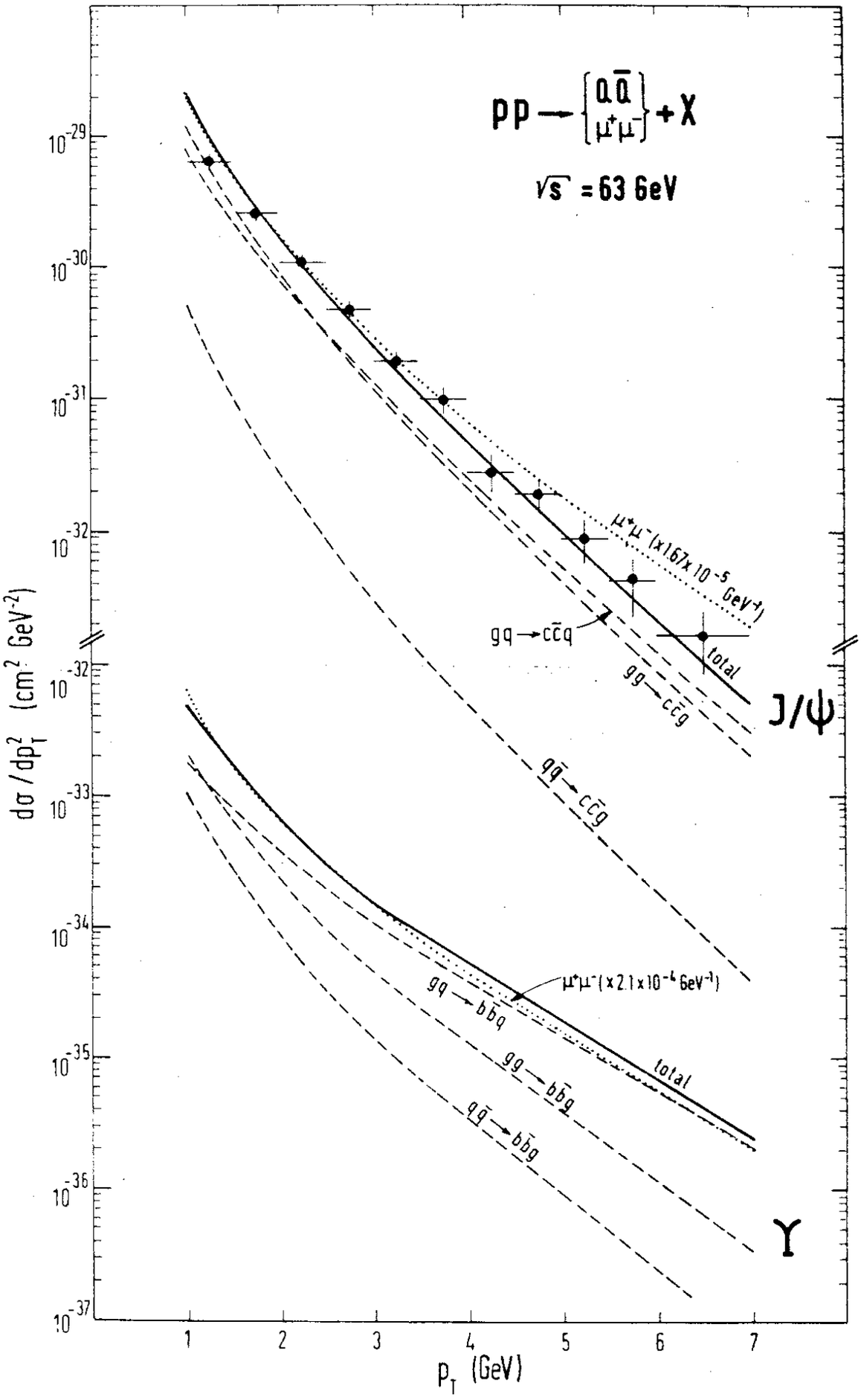
$pp \rightarrow \{q\bar{q}, \mu^+\mu^-\} + X$
$\sqrt{s}$ = 63 GeV
$d\sigma/dp_T^2$ (cm^2 GeV^{-2})
p_T (GeV)
$\mu^+\mu^-$ (x1.67 x 10^{-5} GeV^{-1})
$gq \rightarrow c\bar{c}q$
total
$gg \rightarrow c\bar{c}g$
J/ψ
$q\bar{q} \rightarrow c\bar{c}g$
$\mu^+\mu^-$ (x 2.1 x 10^{-4} GeV^{-1})
$gq \rightarrow b\bar{b}q$
total
$gg \rightarrow b\bar{b}g$
$q\bar{q} \rightarrow b\bar{b}g$
Υ

Fig. 4

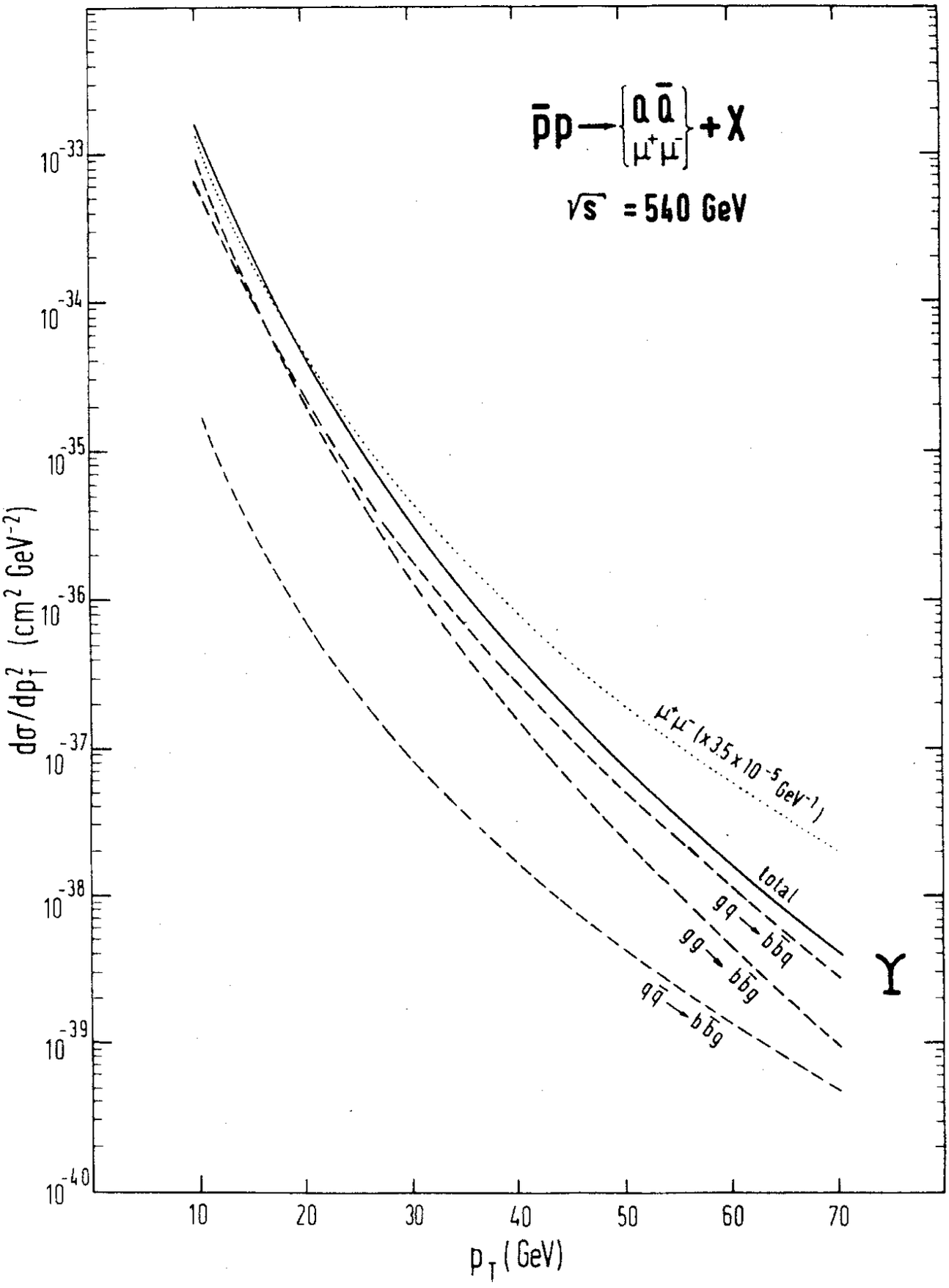
$\bar{p}p \rightarrow \{q\bar{q}, \mu^+\mu^-\} + X$
$\sqrt{s}$ = 540 GeV
$d\sigma/dp_T^2$ (cm^2 GeV^{-2})
p_T (GeV)
$\mu^+\mu^-$ (x 3.5 x 10^{-5} GeV^{-1})
total
$gq \rightarrow b\bar{b}q$
$gg \rightarrow b\bar{b}g$
$q\bar{q} \rightarrow b\bar{b}g$
Υ

Fig. 5

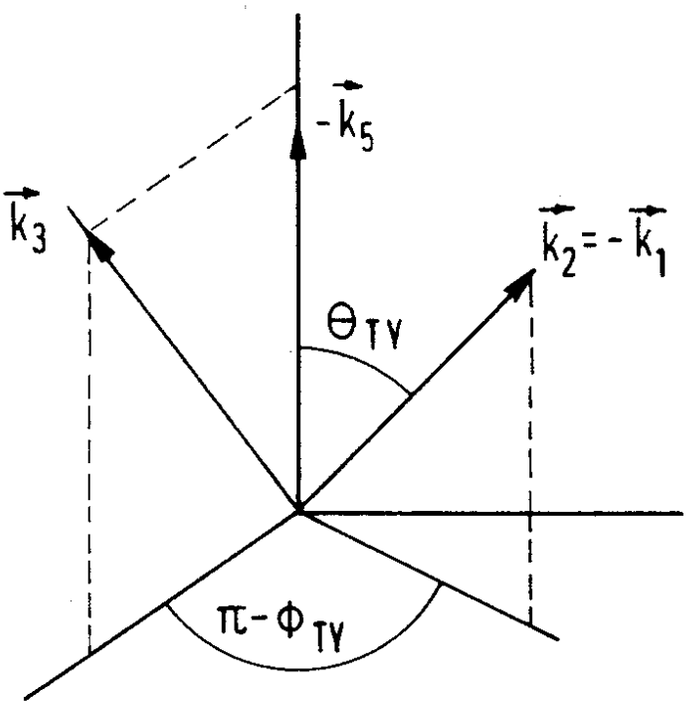

Fig. 6

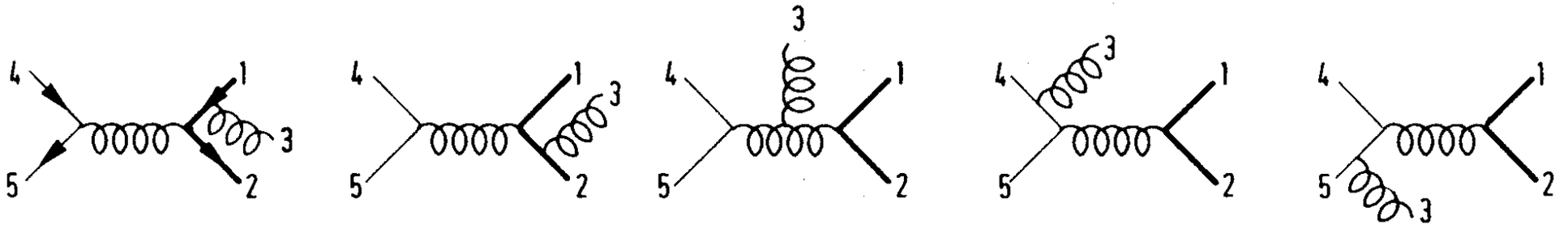

Fig. 7